

Power-Dependent Impedance of High Temperature Superconductor Thin Films: Relation to Harmonic Generation*

James C. Booth[†], L.R. Vale[†], R.H. Ono[†], and J.H. Claassen[‡]

Corr. author: James C. Booth, Mail Stop 814.03, NIST, 325 Broadway, Boulder CO 80303 USA

Abstract – We present measurements of the power-dependent microwave surface impedance of $\text{YBa}_2\text{Cu}_3\text{O}_{7-\delta}$ thin films performed using patterned coplanar waveguide (CPW) resonators at 5.87 GHz and 76 K. We compare these resonator measurements with third-harmonic generation measurements performed on CPW transmission lines of the same geometry patterned onto the same thin-film sample at the same frequency and temperature. We find that the power-dependent surface reactance $X_s(P_{\text{rf}})$ is directly related to the magnitude of the generated third-harmonic signal, indicating a common origin for both of these manifestations of nonlinearity in high-temperature superconductor (HTS) devices. These results are consistent with the nonlinear response generated by a current-dependent penetration depth $\lambda(J)$, which provides a material limitation on the linearity that can be achieved in any practical HTS microwave device.

Keywords: High-temperature superconductor, microwave device, nonlinear response, surface impedance

* This work is a contribution of the U.S. Government, not subject to U.S. copyright.

[†] National Institute of Standards and Technology, Boulder, CO, U.S.A.

[‡] Naval Research Laboratory, Washington, DC, U.S.A.

Microwave devices fabricated from high temperature superconductors offer many performance advantages due to the very low values of surface resistance obtainable in these materials [1]. As a result, high temperature superconductor (HTS) materials are currently being used to build radio receiver filters that have low insertion loss, extremely sharp skirts, and high interference rejection [2],[3]. When combined with cryogenically cooled low-noise amplifiers, HTS filters enable the manufacture of very high performance receiver front ends for wireless base stations [4]. For such telecommunications applications, component linearity is a key concern. Compared to devices fabricated from normal metals, HTS devices have been shown to generate larger nonlinear interference products (higher-order harmonics and intermodulation products), which are undesirable and can ultimately compromise the benefits of using HTS components [1]. Efforts to minimize nonlinear effects have been hampered both by a lack of theoretical understanding of the origin of the nonlinear response in HTS devices and by experimental studies that yield widely varying results in many different device geometries that are difficult to compare quantitatively [5]-[11].

To minimize the nonlinear response of HTS microwave components, it is helpful first to understand the nonlinear response of the HTS material. To address this issue, there has been much recent work [7],[10],[12]-[15] examining the nonlinear (rf power-dependent) surface impedance, since a nonlinear surface impedance will generate nonlinear interference in any practical device. However, there have been relatively few studies that examine both the power-

dependent surface impedance and higher-order harmonic or intermodulation product generation in the same sample (see Ref. [7] for a work that does address both effects). In this work we examine the power-dependent surface impedance [$Z_s(P_{rf}) = R_s(P_{rf}) + iX_s(P_{rf})$, where R_s and X_s are the surface resistance and reactance, respectively] of patterned coplanar waveguide (CPW) resonators using on-wafer probe station measurements and a high power network analyzer. We then compare the $Z_s(P_{rf})$ measurements with third harmonic generation measurements on the same sample, and show that the power-dependent surface reactance $X_s(P_{rf})$ of the CPW resonators is directly related to the magnitude of the generated third-harmonic signal in CPW transmission lines of the same geometry at the same frequency.

We are able to describe the above results in terms of a current-dependent penetration depth $\lambda(J)$ that can be used to quantify the nonlinearity of the HTS material. We find that the form of the current-dependent penetration depth inferred from these microwave measurements agrees well with $\lambda(J_{dc})$ reported on unpatterned HTS films by low-frequency mutual inductance measurements [16]. Knowledge of $\lambda(J)$ enables the comparison of the nonlinear response of different materials, since both the magnitude of generated harmonics and the power-dependent surface impedance depend on the specific geometry of the device studied, and can be meaningfully compared only in identical devices. These measurements therefore demonstrate a direct connection between nonlinear device performance (third harmonic generation in CPW transmission lines) and the power-dependent surface impedance ($Z_s(P_{rf})$ in CPW resonators),

both of which can be described quantitatively by a material-dependent property (current-dependent penetration depth $\lambda(J)$).

2. Power-dependent surface impedance measurements

In order to obtain the power-dependent surface impedance $Z_s(P_{rf})$ of HTS thin films, we use on-wafer measurements of patterned CPW resonators in a cryogenic microwave probe station. We also fabricate a complete multilayer through-reflect-line (TRL) calibration set [17] in the same geometry as the resonator on the same thin-film sample. This allows us to perform on-wafer calibrations and subsequently obtain calibrated S-parameter measurements of the resonator under test. We also use the multiple transmission lines of different lengths in the TRL calibration set to measure third harmonic generation in the same sample as the resonator used in the power-dependent surface impedance measurements.

Our HTS samples are c-axis-oriented thin films (typically 400 nm in thickness, and 10 mm x 10 mm in area) of $\text{YBa}_2\text{Cu}_3\text{O}_{7-\delta}$ (YBCO) grown on LaAlO_3 substrates by pulsed laser deposition. For the measurements described here, we use a CPW geometry with a center conductor linewidth of 21 μm , and a gap spacing (the gap between the center conductor and ground planes on either side) of 40 μm . The CPW resonator is 7.096 mm in length, and coupling is achieved with capacitive gaps of 100 μm in the center conductor. The TRL calibration set consists of a 0.2 mm long through line, three transmission lines of different lengths (from 0.7 mm to 7.744 mm) as well as a short-circuit reflect. The YBCO films typically have a

superconducting transition temperature (measured resistively) of $T_c > 90$ K, and mutual inductance measurements of the penetration depth on a companion sample give $\lambda = 341$ nm at 76 K. Probe station measurements of the CPW resonator at 76 K give a resonant frequency f_0 of 5.87 GHz and an unloaded quality factor Q of 2330. Simulations [18] of this geometry are used to extract a value for the surface resistance at 76 K, scaled to 10 GHz, of $R_s = 440 \mu\Omega$.

Before performing high power measurements, we first make calibrated low-power measurements of the resonator under test at 76 K. We perform a multiline TRL calibration [17] using the calibration artifacts on the same wafer as our resonator. The multiline TRL calibration allows us to eliminate the effects of cabling, microwave probes and contacts, and places the reference plane for the calibrated S-parameter measurements on-chip at the location of the capacitive coupling gaps to the resonator. The reference impedance for the calibrated S-parameter measurements is set to 50Ω by comparison to a TRL calibration of a well-characterized gold calibration set on quartz [19]. Using the on-wafer calibration scheme allows us to accurately measure the insertion loss of the resonator, which is used to determine the average microwave currents flowing in the resonator. We perform the calibration only at low powers – the transmission coefficient measured at high power is simply scaled by the appropriate amount, determined by comparing the transmission coefficient measured with and without the low-power calibrations (see Fig. 1). The TRL calibration also allows us to determine the

characteristic impedance and inductance per unit length of the CPW transmission lines [20], which will be used in the subsequent analysis of $Z_s(P_{rf})$.

In order to perform complex S-parameter measurements at elevated microwave powers, we use a vector network analyzer test set that is specifically modified to enable higher signal powers [21]. Briefly, this test set makes the rf signal accessible at the source so that it can be passed through an external amplifier and back into the test set before the reference signal is sampled. We use this modified test set with a solid state amplifier in order to provide powers up to 23 dBm at the test ports (dBm is not an SI unit; it is related to a power of 1 mW as $10 \log x$, where x is in milliwatts). Typical network analyzer test sets allow powers only up to 0 dBm at the test ports. This modified test set requires isolators to be inserted into the signal path in order to protect the forward/reverse transfer switch from high powers. Since the test set samples the reference signal **after** amplification, it is possible to obtain full complex transmission coefficient data without the need to characterize the gain and phase delay of the amplifier.

Figure 1 shows the magnitude of the transmission coefficient of the 21 μm linewidth resonator measured at 76 K as the incident power is increased from -8 to $+22$ dBm. The power incident on the probe station is measured separately as a function of the internal source power using a power meter, and corrections are made for the insertion loss of the probe station cables and coplanar probes, which is determined from the low power on-wafer calibrations.

Figure 2 shows the relative change in $1/Q$ and resonant frequency f_0 as a function of the incident power. We plot $\Delta(1/Q)$ and Δf_0 because these quantities are proportional to the change in surface resistance and reactance, respectively. The resonant frequency and quality factor are determined from the full complex S_{21} vs. frequency data by a nonlinear least-squares fit to the S_{21} phase vs. frequency data [22]. We believe that this method of extracting Q and f_0 is more reliable than determining these quantities from the magnitude S_{21} data alone, particularly at higher powers. Note from Fig. 2 that the relative change in $1/Q$ is much larger than the relative change in f_0 .

In order to compare our power-dependent resonator measurements with harmonic-generation experiments in a transmission line geometry, we need to calculate the change in the inductance and resistance per unit length of our resonator as a function of the average rf current in the resonator. To accomplish this, we note that the relative change in resonant frequency f_0 and quality factor Q is proportional to the relative change in the inductance ΔL and resistance ΔR per unit length, respectively, of the CPW resonator:

$$\begin{aligned} \frac{\Delta f_0}{f_0} &\approx -\frac{1}{2} \frac{\Delta L}{L} \\ Q \cdot \Delta\left(\frac{1}{Q}\right) &\approx \frac{\Delta R}{R} \end{aligned} \quad (1)$$

To calculate the change ΔR or ΔL (which is required to calculate harmonic and intermodulation product generation) it is necessary to know the total inductance per unit length (L in Eq.(1)).

Once L is obtained, R can be determined from the relation for the unloaded quality factor $Q = \omega L/R$.

We use the calibration comparison technique [19] to obtain the characteristic impedance Z_0 of our CPW transmission lines. The characteristic impedance can be combined with the propagation constant γ determined from the multiline TRL calibration to obtain the distributed circuit parameters R, L, C per unit length [20] as a function of frequency for the 21 μm wide transmission lines, under the assumption that the conductivity per unit length of the transmission lines can be neglected. Figure 3(a) shows the measured (low-power) inductance per unit length at 76 K, along with the results of a calculation [23] for $L(\omega)$ using the transmission line geometry and the measured penetration depth. The total resistance per unit length R can in principle also be determined by the same calibration comparison method, but in practice it is difficult to obtain with transmission line measurements because R is small compared to the other circuit parameters ωL and $1/\omega C$. Figure 3(b) shows the real part of the characteristic impedance Z_0 , which will be used below to help determine the average current in the resonator.

In addition to determining ΔR and ΔL from the relative change in Q and f_0 , it is also necessary for the calculation of harmonic and intermodulation product generation to determine the average current in the resonator from the measured incident microwave power. We note that for a resonator of length l the current flowing in mode n is given by [24]

$$I(z) = I_0 \sin\left(\frac{n\pi z}{l}\right) , \quad (2)$$

where z is the direction along the length of the resonator. The peak current I_0 is given by

$$I_0 = \sqrt{\frac{r_v(1-r_v)8QP}{n\pi Z_0}} \quad , \quad (3)$$

where Q is the unloaded quality factor, Z_0 is the characteristic impedance, P is the incident power, and r_v is the voltage insertion ratio, which is related to the insertion loss IL by $IL = -20\log(r_v)$. In order to compare the $Z_s(P_{rf})$ results measured in a resonator geometry with harmonic generation measured in a transmission line geometry, we need to calculate the average rf current I_{avg} , defined by

$$I_{avg} = \frac{\int_0^1 I(z) dz}{\int_0^1 dz} \quad . \quad (4)$$

Using Eqs. (2) and (3) in Eq. (4) we obtain the following relation between the average current and the incident power:

$$I_{avg} = \frac{2}{\pi} \sqrt{\frac{r_v(1-r_v)8Q_c P}{n\pi Z_0}} \quad . \quad (5)$$

In Eq. (5), the quantities r_v , Q , and Z_0 are all experimentally determined. We determine Z_0 at the resonant frequency by the calibration comparison technique, which was described previously for determining the total inductance per unit length L (see Fig. 3(b)). The quantity r_v is determined from the insertion loss, which we are able to determine accurately from our calibrated S-parameter measurements of the resonator under test. In principle, all of these quantities also

change as the power is increased; in practice we measure the Q and insertion loss as a function of incident power, but we assume that the characteristic impedance Z_0 does not change significantly with increasing power. In this manner we are able to determine the average current flowing in the resonator from the measured incident power.

Figure 4 shows the rf-current dependent quantities $\Delta R(I)$ and $\Delta L(I)$, which are respectively the resistance per unit length and the inductance per unit length, at a frequency of 5.87 GHz and a temperature of 76 K. It can be seen from this figure that the nonlinear contribution from the reactance is larger than that from the resistance for virtually all measured powers. This is to be expected for a superconducting transmission line, where the linear reactance per unit length ωL is much larger than the linear resistance per unit length R . Note that the resistance and reactance per unit length for the CPW transmission lines are related to the surface resistance and surface reactance for the thin film by a simple geometry factor [18]. However, it is the resistance and inductance per unit length that are the relevant quantities for calculating harmonic and intermodulation product generation in transmission lines. In order to quantify the nonlinear inductance, we fit $L(I)$ in Fig. 4 to a quadratic form $L(I) = L_0 + L'I^2$, and we obtain for the nonlinear coefficient $\omega L' = 934 \text{ } \Omega/(\text{A}^2 \cdot \text{m})$. It is this quantity that we will compare with harmonic generation results in our CPW structures. The determination of $\omega L'$ from the data in Fig. 4 depends sensitively on what portion of the data is included in the

quadratic fit—the extracted value of $\omega L'$ ranges from 980 to 803 $\Omega/(A^2 \cdot m)$ as more or less data are included in the fit.

3. Third harmonic and intermodulation product generation

Once we obtain the nonlinear contribution to the resistance and inductance per unit length for our CPW transmission lines, we should be able to directly calculate the magnitude of the higher harmonics and intermodulation products generated by this nonlinear impedance. In what follows, we will calculate the third-order harmonics and intermodulation products generated by the nonlinear inductance shown in Fig. 4. Although practically it is the third-order intermodulation products that are of concern in actual applications, we show below that the third-order intermodulation products and third harmonics are very closely related. We will for now ignore the nonlinear resistance $\Delta R(I)$ since it is smaller than $\omega \Delta L$ for all measured powers. We will then compare the calculated magnitude of the third-harmonic signal with measurements of third-harmonic generation in the CPW transmission lines of variable length that make up the TRL calibration set on the same chip as the resonator discussed earlier.

We have previously calculated [25] the magnitude of the third harmonic signal generated by a nonlinear inductance (per unit length) of the form

$$L(I) = L_0 + \Delta L(I) = L_0 + L' I^2 \quad . \quad (6)$$

We repeat the calculation here using the value for $L(I)$ determined from Fig. 4. We begin by calculating the voltage across the inductor of length l described by Eq. (6):

$$V(t) = \mathbb{1}L \frac{dI(t)}{dt} = \mathbb{1}L_0 \frac{dI}{dt} + \mathbb{1}L' I^2 \frac{dI}{dt} . \quad (7)$$

For the driving current we assume a two-tone stimulus of the form

$$I(t) = I_1 \cos(\omega_1 t) + I_2 \cos(\omega_2 t) . \quad (8)$$

We now substitute Eq. (8) into Eq. (7) and calculate the voltage generated by the nonlinear term

in Eq. (7). The full expression for the nonlinear contribution to the voltage $V(t)$ is given by

$$\Delta V(t) = -\frac{\mathbb{1}L'}{4} \left\{ \begin{array}{l} \omega_1 (I_1^3 + 2 I_1 I_2^2) \sin(\omega_1 t) + \omega_2 (I_2^3 + 2 I_1^2 I_2) \sin(\omega_2 t) \\ + \omega_1 I_1^3 \sin(3\omega_1 t) + \omega_2 I_2^3 \sin(3\omega_2 t) \\ + I_1 I_2^2 (2\omega_2 + \omega_1) \sin((2\omega_2 + \omega_1)t) + I_1 I_2^2 (2\omega_2 - \omega_1) \sin((2\omega_2 - \omega_1)t) \\ + I_1^2 I_2 (2\omega_1 + \omega_2) \sin((2\omega_1 + \omega_2)t) + I_1^2 I_2 (2\omega_1 - \omega_2) \sin((2\omega_1 - \omega_2)t) \end{array} \right\} . \quad (9)$$

Note from Eq. (9) that the coefficients of the third harmonic terms ($\sin 3\omega_1 t$, $\sin 3\omega_2 t$) are identical to the coefficients of the third-order intermodulation terms ($\sin(2\omega_2 - \omega_1)$, $\sin(2\omega_1 - \omega_2)$) at their respective frequencies, if the drive signals are the same ($I_1 = I_2$).

If we now consider the case of just a single input tone at frequency ω_1 , the generated third harmonic signal at frequency $3\omega_1$ is given by

$$V_{3\omega} = \frac{\mathbb{1}\omega_1 L' I_1^3}{4} \sin(3\omega_1 t) . \quad (10)$$

In order to compare with measurements of third-harmonic generation, we need to calculate the power generated at frequency $3\omega_1$ in a transmission line of characteristic impedance Z_0 :

$$P_{3\omega} = \frac{V \cdot V^*}{2Z_0} = \frac{1}{2Z_0} \left[\frac{\mathbb{1}\omega L' I_1^3}{4} \right]^2 . \quad (11)$$

If we make the identification that the power in the fundamental is given by $P_1 = I_1^2 \cdot Z_0 / 2$, then we can write the expression for $P_{3\omega}$ in terms of P_1

$$P_3 = \left[\frac{\omega L' 1}{2Z_0^2} \right]^2 P_1^3 \quad . \quad (12)$$

If we now take the logarithm of Eq. (12) we obtain

$$\log P_3 = 2 \log \left[\frac{\omega L' 1}{2Z_0^2} \right] + 3 \log P_1 \quad . \quad (13)$$

Equation (13) says that if we plot the magnitude of the generated third-harmonic signal as a function of the power in the fundamental on a log-log plot, we should observe a straight line of slope three with an intercept specified by the first term in Eq. (13). For third-harmonic measurements one typically specifies the third-order intercept point IP_3 , which is related to the y-intercept b on the log-log plot by $\log IP_3 = -(b/2)$. This specification of the third-order intercept point gives the power in the fundamental where the line of slope 3 (describing the third harmonic) would intercept a line of slope 1 and intercept 0 (describing the power in the fundamental). We can obtain a value for IP_3 for the nonlinear inductor from Eq. (13):

$$\log IP_3 = \log \frac{2Z_0^2}{\omega L' 1} \quad . \quad (14)$$

This expression gives us a measurable quantity (IP_3) in terms of the parameter $\omega L'$, which we determined previously from the power-dependent resonator measurements. Conversely, we can analyze third-harmonic generation data to extract a value for $\omega L'$ to compare with the value obtained from the resonator measurements. We can therefore compare the results of our power-

dependent resonator measurement with third-harmonic measurements by measuring the third order intercept IP_3 .

Our measurements of third-harmonic generation are described in Ref. [25]. For CPW transmission lines in the cryogenic probe station, we measure the transmitted power in the fundamental at frequency f , the second harmonic at frequency $2f$, and the third harmonic at frequency $3f$, all as functions of incident power. We determine any background contributions for the second and third harmonics by measuring a normal metal (silver) transmission line at cryogenic temperatures. For the powers used for the superconducting transmission lines, we see no measurable background third harmonic, although a background second harmonic appears at the highest input powers, just above our noise threshold, which is approximately -130 dBm.

Figure 5 shows the generated third harmonic signal as a function of the power in the fundamental for four transmission lines of different lengths at $f = 5.87$ GHz and $T = 76$ K. All of the transmission lines have the same nominal geometry as the resonator discussed previously. Immediately apparent from Fig. 5 is that the measured power in the third harmonic increases with a slope 3 on the log-log plot as predicted by Eq. (13) for all of the lines measured. This makes it possible to describe the third-harmonic data for each transmission line by specifying its third-order intercept point IP_3 . The inset to Fig. 5 shows the third-order intercepts IP_3 plotted as a function of line length. The solid line shows a fit to the data using Eq. (14), where we have allowed the parameter L' and a length offset to vary. (We allow the length to vary in the fit

because all of our 21 μm transmission lines include a tapered section that transforms from a probe-compatible geometry to the desired 21 μm geometry. Therefore the measured third-order intercepts should be analyzed as a function of the difference in line lengths, not absolute lengths.) We observe no second-harmonic signal within the resolution of our measurement system for the four transmission lines measured.

From the fit to the IP_3 data in Fig. 5, we obtain $\omega L' = 825 \text{ } \Omega/(\text{A}^2 \cdot \text{m})$, which compares favorably with the value obtained from the power-dependent resonator measurements, $\omega L' = 934 \text{ } \Omega/(\text{A}^2 \cdot \text{m})$. An uncertainty in the fit given in Fig. 5 of $\pm 0.5 \text{ dBm}$ gives a range of values for $\omega L'$ of $735 - 925 \text{ } \Omega/(\text{A}^2 \cdot \text{m})$. The differences in the two determinations of $\omega L'$ could be due to errors in the experimental determinations of these quantities, or could reflect detailed differences between the resonator and transmission line geometries used in the respective measurements. Nevertheless, the demonstration of the quantitative agreement between these two different determinations of the nonlinear response for an HTS microwave device is significant.

4. Determination of $\lambda(\mathbf{J})$

While the above comparison shows very good agreement between the two different measures of nonlinear effects in HTS devices, the quantity $\omega L'$ is specific to the geometry of the transmission lines and resonators studied. In order to compare the nonlinear response of our YBCO material to that of other materials, it would be helpful to specify the magnitude of the nonlinear response in terms of a material property. This can be accomplished by noting that a

nonlinear inductance of the form of Eq. (6) can be generated by a current-dependent penetration depth of the form [26]

$$\lambda^2(T, J) = \lambda^2(T) \left[1 + \left(\frac{J}{J_0(T)} \right)^2 \right] . \quad (15)$$

The parameter J_0 is the nonlinear scaling current density, and quantifies the nonlinearity of the superconductor. We calculate the inductance per unit length from the expression [26]

$$L = \frac{\mu_0 \int (H^2 + \lambda^2 J^2) dS}{\left(\int J dS \right)^2} , \quad (16)$$

where the integration is carried out over the cross-section of the planar transmission line.

Substituting Eq. (15) into Eq. (16), we obtain for the nonlinear contribution to the inductance

$$L' = \frac{\mu_0 \lambda^2(T) \Gamma'}{J_0^2} , \quad (17)$$

where Γ' is a geometrical factor given by

$$\Gamma' = \frac{\int J^4 dS}{\left(\int J dS \right)^4} . \quad (18)$$

The geometrical factor Γ' can be calculated if the current distribution for the planar circuit used is known. For the CPW geometry investigated here, we use a numerical calculation [23] to determine the current density at 76 K, and then determine Γ' based on Eq. (18).

Once we have calculated the geometry factor Γ' , we can use Eqs. (17) and (18) to calculate the material parameter J_0 from both of the microwave frequency experiments described

above. From the power-dependent resonator measurements, we obtain $J_0 = 21 \text{ MA/cm}^2$, based on $\omega L' = 934 \text{ } \Omega/(\text{A}^2 \cdot \text{m})$. From the third-order intercept measurements, we obtain $J_0 = 22 \text{ MA/cm}^2$, based on $\omega L' = 825 \text{ } \Omega/(\text{A}^2 \cdot \text{m})$. These values of J_0 agree well with values of J_0 for YBCO thin films determined by mutual inductance measurements and reported in Ref. [16].

5. Conclusions

In conclusion, we have demonstrated a technique by which we are able to measure the power-dependent surface impedance of superconducting YBCO thin films in a patterned CPW resonator. The degree of nonlinearity is determined by measuring the nonlinear contribution to the transmission line inductance. The degree of nonlinearity extracted from the power-dependent resonator measurements agrees well with same quantity extracted from third-harmonic measurements of CPW transmission lines of the same geometry at the same frequency and temperature. Furthermore, both microwave frequency results are consistent with a model based on nonlinearity arising due to a current-dependent penetration depth. We believe that these two different determinations of the nonlinearity of HTS thin films will contribute toward determining a limit on the linearity of general HTS microwave devices, and could also facilitate the further minimization of the nonlinear response of HTS materials.

Acknowledgements

This work was supported in part by the Office of Naval Research. We thank J.A. Beall and D.C. DeGroot for helpful comments.

References

- [1] Z. Y. Shen, *High-Temperature Superconducting Microwave Circuits* (Artech House, Boston, 1994).
- [2] R.S. Kwok *et al.*, IEEE Trans. Microwave Theory Tech. **47**, 586 (1999).
- [3] G.-C. Liang *et al.*, IEEE Trans. Microwave Theory Tech. **43**, 3020 (1995).
- [4] Z. Ma *et al.*, Extended Abstracts of 6th Int. Supercond. Electron. Conf., Vol.1, 128 (1997).
- [5] J.P. Hong, and J.S. Lee, Appl. Phys. Lett. **68**, 3034 (1996).
- [6] Y. Yoshitake, S Tahara, and S. Suzuki, Appl. Phys. Lett. **67**, 3963 (1995).
- [7] Z. Ma *et al.*, IEEE Trans. Applied Supercond. **7**, 1911 (1997).
- [8] B.A. Willemsen, T. Dahm, and D.J. Scalapino, Appl. Phys. Lett. **71**, 3898 (1997).
- [9] G. Hampel *et al.*, Appl. Phys. Lett. **71**, 3904 (1997).
- [10] R.R. Mansour *et al.*, IEEE Trans. Microwave Theory Tech. **44**, 1322 (1996).
- [11] H. Hoshizaki, N. Sakakibara, and Y. Ueno, J. Appl. Phys. **86**, 5788 (1999).
- [12] D. E. Oates *et al.*, J. Supercond. **8**, 725 (1995).
- [13] J.R. Powell *et al.*, J. Appl. Phys. **86**, 2137 (1999).
- [14] J. Halbritter, Supercond. Sci. Technol. **12**, 883 (1999).
- [15] A.P. Kharel *et al.*, Phys. Rev. B **58**, 11189 (1998).
- [16] J.H. Claassen *et al.*, Appl. Phys. Lett. **74**, 4023 (1999).
- [17] R.B. Marks, IEEE Trans. Microwave Theory Tech. **39**, 1205 (1991).

- [18] James C. Booth and C.L. Holloway, *IEEE Trans. Microwave Theory Tech.* **47**, 769 (1999).
- [19] R.B. Marks, J.A. Jargon, and J.R. Juroshek, 48th ARFTG Conference Digest, p. 38–45 (1996).
- [20] R.B. Marks and D.F. Williams, *IEEE Trans. Microwave Guided Wave Lett.* **3**, 247 (1993).
- [21] C. Wilker *et al.*, 47th ARFTG Conference Digest, p. 32-41, (1996).
- [22] For a detailed description of this and other methods for determining resonator Q, see P.J. Petersan and S.M. Anlage, *J. Appl. Phys.* **84**, 3392 (1998).
- [23] D.M. Sheen *et al.*, *IEEE Trans. Appl. Superconductivity* **1**, 108 (1991).
- [24] D.E. Oates, A.C. Anderson, and P.M. Mankiewich, *J. Supercond.* **3**, 251 (1990).
- [25] James C. Booth *et al.*, *J. Appl. Phys.* **86**, 1020 (1999).
- [26] T. Dahm and D.J. Scalapino, *J. Appl. Phys.* **81**, 2002 (1997).

Figure Captions

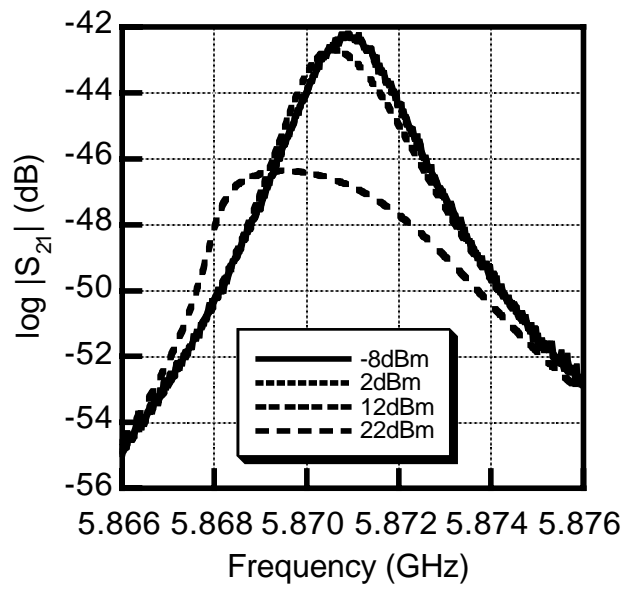
Fig. 1. Magnitude of transmission coefficient S_{21} vs. frequency, for a YBCO coplanar waveguide resonator at 76 K, for increasing microwave power. The S_{21} curve measured at low power is corrected using an on-wafer TRL calibration scheme.

Fig. 2. Relative change in (a) the resonant frequency and (b) the quality factor of a YBCO coplanar waveguide resonator at 76 K as a function of incident microwave power.

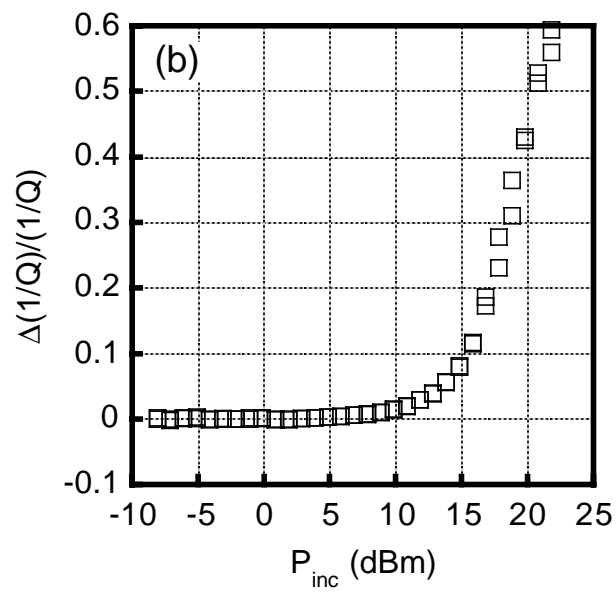
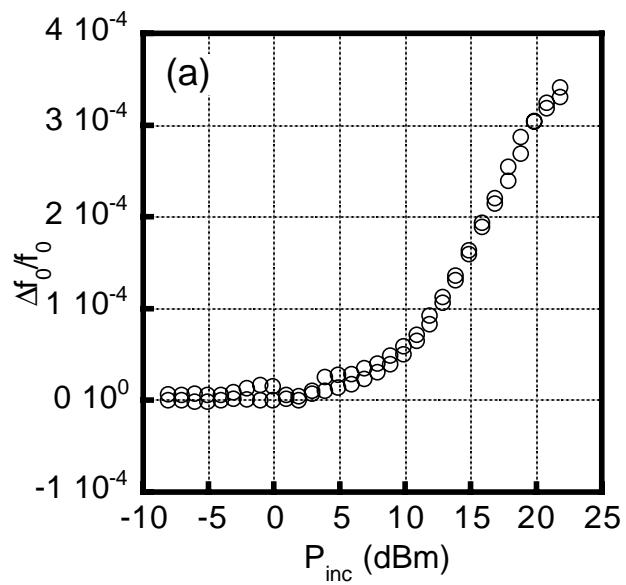
Fig. 3. Frequency dependence of (a) the inductance per unit length and (b) real part of the characteristic impedance of YBCO coplanar waveguide transmission lines at 76 K.

Fig. 4. Nonlinear contribution to the resistance and reactance per unit length calculated from the power-dependent resonator measurements at 5.87 GHz. Both quantities are plotted as a function of the average rf current flowing in the resonator. The solid line is a quadratic fit to the current-dependent nonlinear reactance.

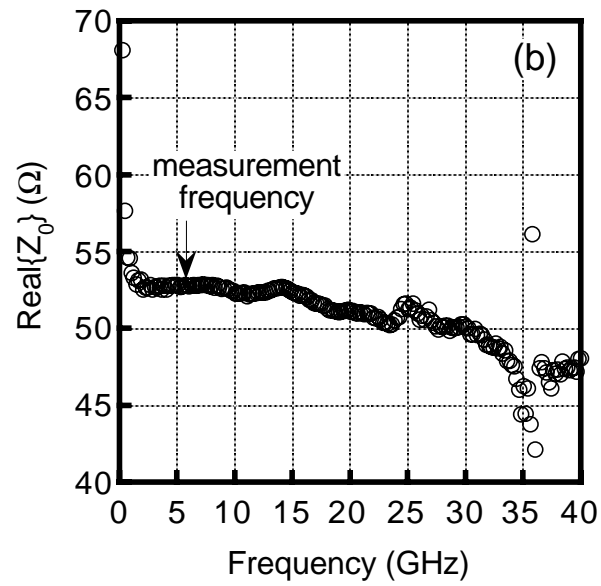
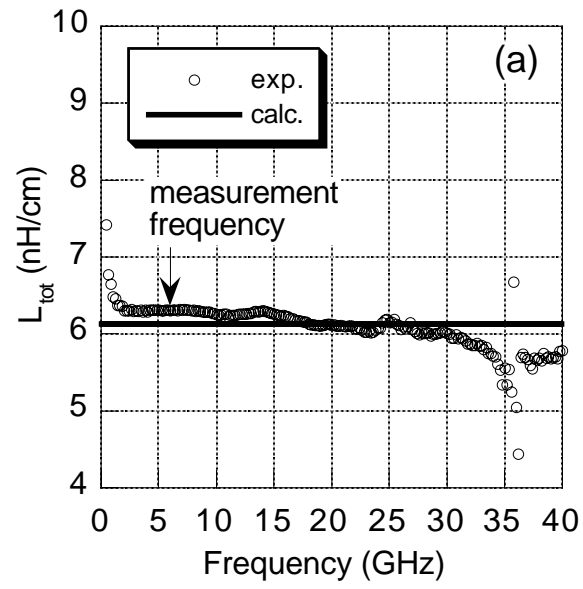
Fig. 5. Measured power in the third-harmonic signal as a function of power in the fundamental signal for four YBCO coplanar waveguide transmission lines of different length at 76 K. Data is shown for lines of length 0.704 mm (circles), 1.96 mm (diamonds), 3.08 mm (squares), and 7.744 mm (x's). The solid line shows a fit to a line of slope three for the 7.744 mm line. The inset shows the third-order intercept IP_3 plotted as a function of line length. The solid line in the inset is a fit to the length dependence given in Eq. (14).



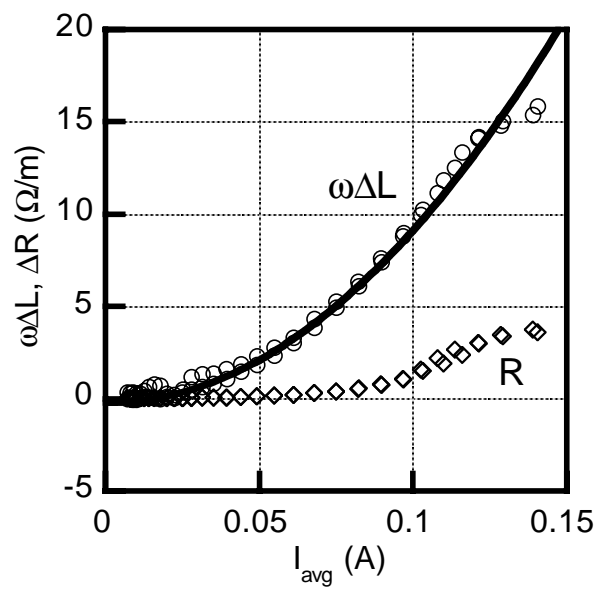
Booth et al., Fig. 1



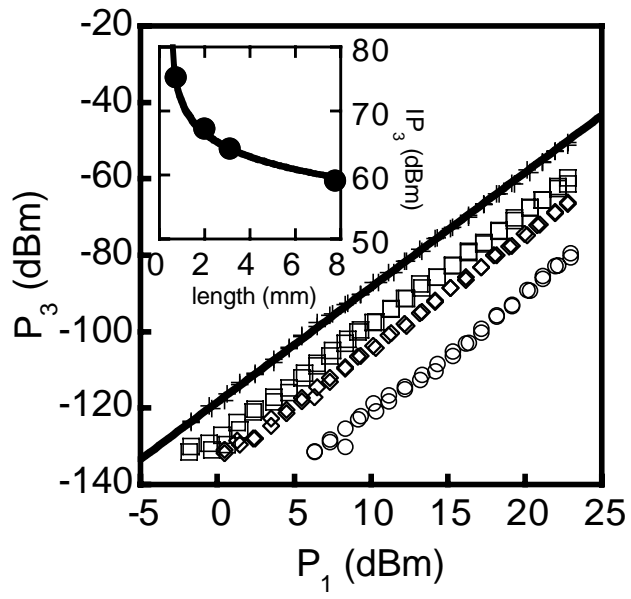
Booth et al., Fig. 2



Booth et al., Fig. 3



Booth et al., Fig. 4



Booth et al., Fig. 5